Journal of the European Ceramic Society 20 (2000) 2377–2387

Densification behaviour and mechanisms of synthetic hydroxyapatites

E. Landi, A. Tampieri *, G. Celotti, S. Sprio

IRTEC-CNR, via Granarolo, 64 - 48018 Faenza, Italy

Received 27 November 1999; received in revised form 2 May 2000; accepted 11 May 2000

Abstract

Starting from $Ca(OH)_2$ and H_3PO_4 hydroxyapatite powders with three different crystallinity degrees have been prepared and characterized. Densification extent and mechanisms were studied through dilatometric measurements in isothermal regime in the range of temperature 750–1250°C: the influence of different powder features (including the effect of calcination treatment) have been evaluated. Powder characterized by the lowest crystallinity degree has the highest densification extent; overlapping phenomena occurring during the sintering treatments are responsible for unexpectedly low values found for the shrinkage rate, which can easily lead to a misidentification of the rate controlling mechanism. An interpretation of the densification mechanism, consistent with all experimental findings, is proposed.

Keywords: Apatite; Densification; Hydroxyapatite; Powders-chemical preparation; Sintering

1. Introduction

Sinterability and mechanical properties of dense hydroxyapatite (HA) are strictly linked to the characteristics of starting HA powder, first among those: particle size, crystallinity and chemical substitutions. In fact Ca/P molar ratio has to be very near to the theoretical one (1.67) in order to avoid chemical substitutions which affect densification behaviour.

Data in literature concerning the thermal decomposition of HA during sintering are still ambiguous as regards the minimum decomposition temperature, as well as the actual extent and products of the decomposition itself. Some results show that stoichiometric hydroxyapatite is stable in dry or moist air up to 1200°C and does not decompose;[1–4] other authors report that stoichiometric HA, after a dehydroxylation process (which occurs gradually but in two steps, i.e. at about 900°C and at 1300–1400°C), starts to decompose into secondary phases at temperature in the range 1350–1500°C.[5–6]

Moreover, it has been already reported that when Ca/P molar ratio exceeds the theoretical value, CaO forms during sintering[7] and in this case the presence of CaO is found to decrease strength and produce decohesion of the whole material due to stresses caused by the formation of $Ca(OH)_2$, which subsequently transforms into $CaCO_3$ with related volume changes.[7–11] If the Ca/P molar ratio of HA is lower than 1.67, β- or α-tricalcium phosphate (TCP) may form[12–16] and its presence increases slow crack growth susceptibility and biodegradability of the HA ceramics.

In that case, the decomposition of HA in air at high temperature hinders sintering and causes decrease in the density.

On the other hand, deviation from the theoretical Ca/P ratio does not necessarily imply the presence of TCP,[17] in fact the existence of chemical substitution as HPO_4^{2-} instead PO_4^{3} and CO_3^{2-} instead of PO_4^{3-} and/or OH cause similar deviation in the Ca/P ratio.[18,19]

Carbonate ions CO_3^{2-} (very common as a contaminant in low crystallinity HA), are reported to not affect the grain growth and to enhance sinterability of HA ceramics if they replace only phosphate groups in the HA lattice. On the other hand, CO_3^{2-} for OH^- substitution has no effect on sintering.

In the present paper, different sintering tests were carried out on samples prepared with different HA powders: dilatometric evaluations were performed in

* Corresponding author.
E-mail address: irtec@irtec1.irtec.bo.cnr.it (A. Tampieri).

0955-2219/00/$ - see front matter
PII: S0955-2219(00)00154-0

the range 750–1250°C in static air, kinetic data and mechanisms evaluations were deduced.

2. Experimental

HA powders were prepared using $Ca(OH)_2$, 95% pure diluted in H_2O, and H_3PO_4 85% pure (Aldrich) diluted in H_2O, following the reaction: $5Ca(OH)_2 + 3H_3PO_4$-$Ca_5(PO_4)_3OH + 9H_2O$. The aqueous solution was continuously stirred. By varying the temperature of the solution between 35 and 95°C, and the ripening time, it was possible to change continuously the degree of crystallinity of the product between 20 and 80%. Batches of powders with crystallinity degree $X_c \approx 20$, 40 and 80% were prepared using a precipitation temperature of 35, 70 and 95°C, respectively. Ripening time of 2 h was used to produce HA powders with low and medium crystallinity degree while the production process of high crystallinity powder involved 24 h of ripening. In any case pH of the liquid phase was controlled and kept at pH≈6.5 for powders A and B and at pH≈7.5 for powder C; then the precipitate was washed, filtered and lyophilised for 48 h. The obtained powder was sieved at 400 and 150μm and its crystallinity degree controlled. Finally, the powder was uniaxially cold pressed at 1000 kg/cm^2; the bars were coded HA-A, HA-B and HA-C in function of the powder used for the preparation (A: $X_c = 80\%$, B: $X_c = 40\%$, C: $X_c = 20\%$). Powder labeled AI was calcined at 800°C for 1 h in static air.

The shrinkage of the green compacts (uniaxially pressed at 1000 kg/cm^2) in function of temperature was measured with horizontal dilatometer (Netzsch Geratebau 402 E) at a heating rate of 5°C/min. Isothermal measures of densification were also performed at various temperatures in the range 750–1250°C with a heating rate of 30°C/min to minimize the reaction advancement during heating.

Dilatometric data were elaborated via software in order to have the sintering behaviour in terms of density change. Shrinkage data manipulation was automatically done by the evaluation program of the dilatometer, starting from the green density of the tested bars (calculated by geometrical method), and the theoretical density of the material (i.e. 3.16 g/cm^3).

Specific surface area of starting powders was evaluated by the BET method (Sorptomatic, Carlo Erba). For particle size distribution measurement, the starting powders were analysed by a sedigraph (Model 5100, Micromeritics Instrument Corp.) after exciting them ultrasonically for 10 min. In order to evaluate Ca/P ratio, ICP analysis was performed by Varian Liberty 200 apparatus.

X-ray diffractometric analysis (Cu$K\alpha$ radiation, Rigaku Miniflex) was used to determine crystalline phases composition of the powders and of dense samples and HA crystallization features. Morphologic evaluation of powders and dense samples was performed by SEM (Leica, Cambridge).

3. Results and discussion

3.1. Characteristics of powders

By controlling the temperature during precipitation and ripening time, powders with three different values of crystallinity degree were produced: powder A = 80%, powder B = 40% and powder C = 20%. The crystallinity degree, corresponding to the fraction of crystalline phase present in the examined volume, was evaluated by the relation:

$$X_c \approx 1 - (V_{112/300}/I_{300})$$

where I_{300} is the intensity of (300) reflection and $V_{112/300}$ is the intensity of the hollow between (112) and (300) reflections, which completely disappears in non-crystalline samples. Being this method sensible to the crystallite dimensions too, a verification can be done with the relation:

$$B_{002}\sqrt[3]{X_c} = K$$

where K is a constant found equal to 0.24 for a very large number of different HA powders, and B_{002} is FWHM (°) of reflection (002). The two above relations give the same result for X_c within 10% in the great majority of practical cases.

XRD analysis of powders revealed no secondary phases besides HA (Fig. 1); from ICP analysis the Ca/P ratio calculated by the respective oxides ratio was ≈1.66 for powder A, ≈1.601 for powder B and ≈1.565 for powder C.[20]

The presence of defective HA [usually expressed as $Ca_{10-x}(PO_4)_{6-x}(HPO_4)_x(OH)_{2-x}$] can be inferred as responsible of the reduction of Ca/P ratio.[4,12,13,20] In fact, FTIR spectra pointed out the presence of HPO_4^{2-} group in powder C, less pronounced in powder B and absent in powder A, respectively. Moreover, the O–H stretch band around 3450 cm^{-1} is more accentuated and shifted at lower frequency in powder C characterized by a higher solvation extent. On the other hand, the presence of the CO_3^{2-} group also proved the formation in powder B of some amount of carbonate-apatite (CO_3^{2-} substituted in both positions OH^- and PO_4^{3-}).

By thermogravimetric analysis, the contributes of the different chemical substitutions in the three powders were settled:[20] at $T \leqslant 200$°C the weight loss is ~6, 2.8 and 1% of powder C, B and A, respectively, due to the different extent of the surface solvation and hydration. On the other hand at $T \geqslant 800$°C weight loss is ~1.8%

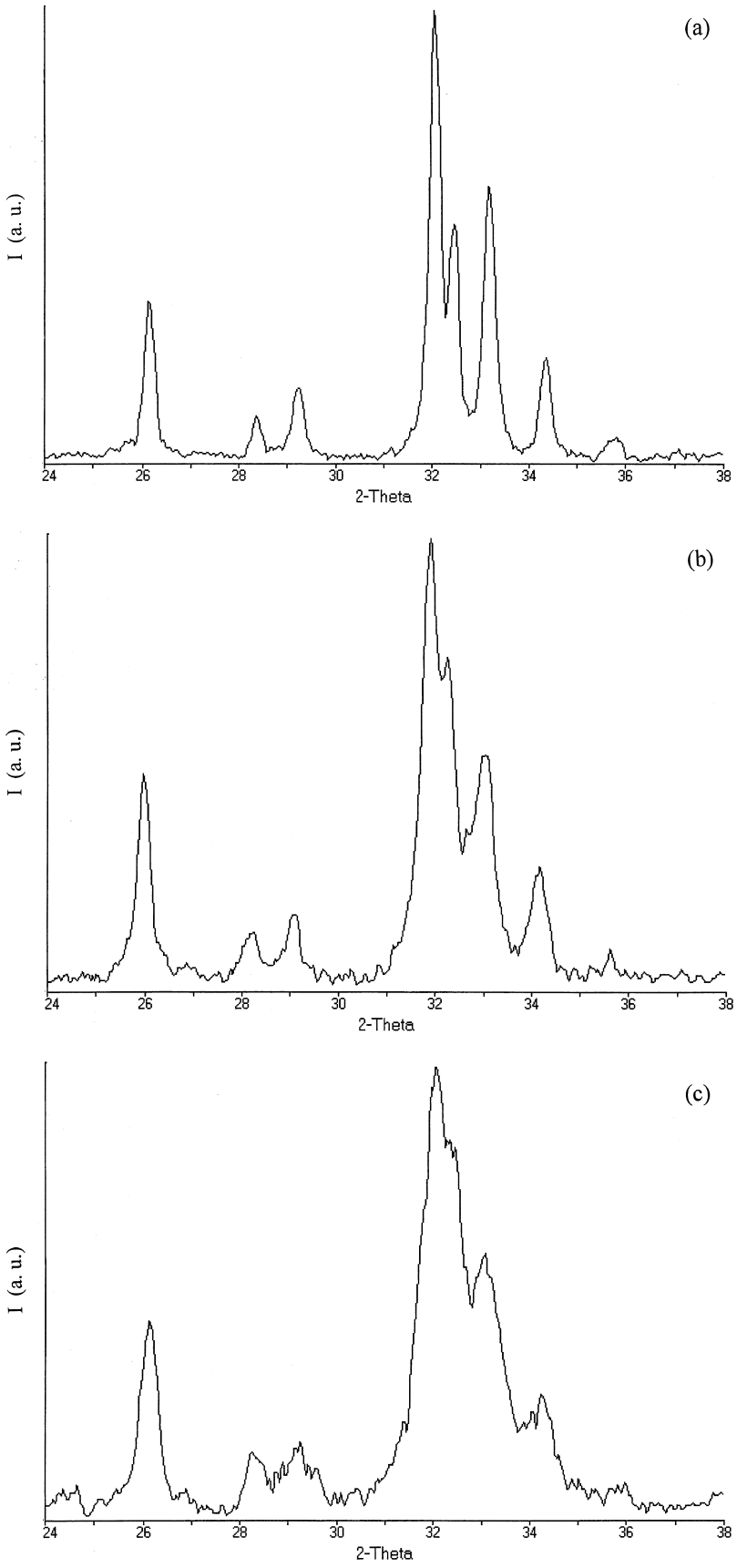

Fig. 1. XRD analysis of HA starting powders showing no secondary phases: high (a), medium (b) and low (c) crystallinity degree.

for powder C and A (i.e. equal to the theoretical one due to dehydroxylation) while it is ~4% for powder B, that is increased by the simultaneous elimination of CO_3^{2-} groups.[20]

The presence of HPO_4^{2-} and CO_3^{2-} groups substituting PO_4^{3-} and OH^- groups simultaneously and in different proportions is responsible for the Ca/P ratio deviation in powders B and C, even if no contaminating calcium phosphate phases were detected.[20]

The morphology of powder A, B and C is shown in Fig. 2a–c which is in agreement with particle size distribution determined by sedimentography:[20] powders B and C are characterized by larger agglomerates (3–4 μm) in turn formed by smaller primary particles (20–30 nm) in respect to powder A, in which grains are smaller but built by larger particles. The specific surface area of the three powders results ≈90, 45 and 15 m^2/g for C, B and A, respectively.

As expected the compaction behaviour of the powders is different: higher green density was obtained with powder A and AI.

3.2. Sintering behaviour and kinetic evaluation

The linear shrinkage of HA-A, HA-B and HA-C green compacts (the last letters represents the used powder), measured by dilatometry from room temperature to 1300–1350°C at a constant heating rate (5°C/min), is reported in Fig. 3. It indicates that sintering begins at lower temperature (820°C) for HA-C and the total shrinkage (≈28%) is larger if compared with HA-A, whose curve shows a sharp fall at ≈900°C and records a total dimension change of ≈22%. HA-B shows an intermediate behaviour: the profile of the curve resembles that of powder C even if the total shrinkage is comparable to that of powder A.

In spite of the dimension of agglomerates, the packing efficiency is influenced by primary particle sizes: green density rises increasing the dimension of primary particles and thus following the order A≈AI > B > C; on the other hand during the heating up to 1300°C HA-C shows higher densification extent in respect to HA-A as expected for powder characterized by smaller and more reactive particles.[21]

The densification curves present a sigmoidal shape with an inflection point around 1100°C shifted at 1150°C

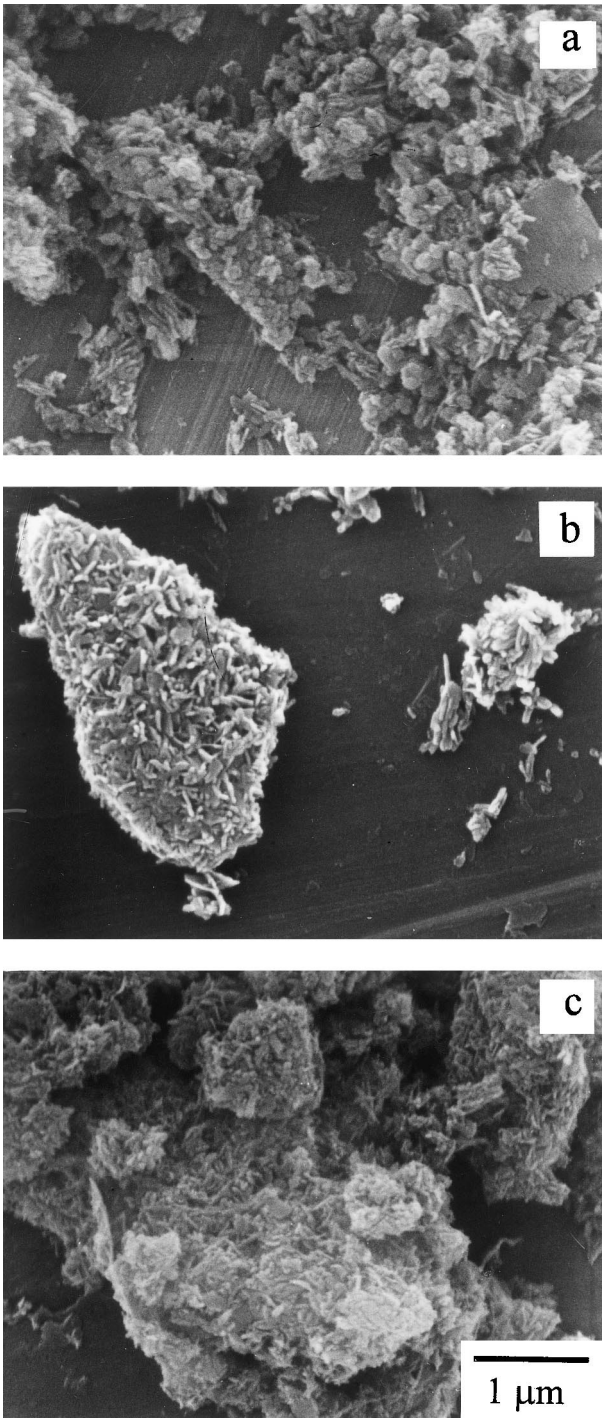

Fig. 2. Morphology of HA starting powders: high (a), medium (b) and low (c) crystallinity degree.

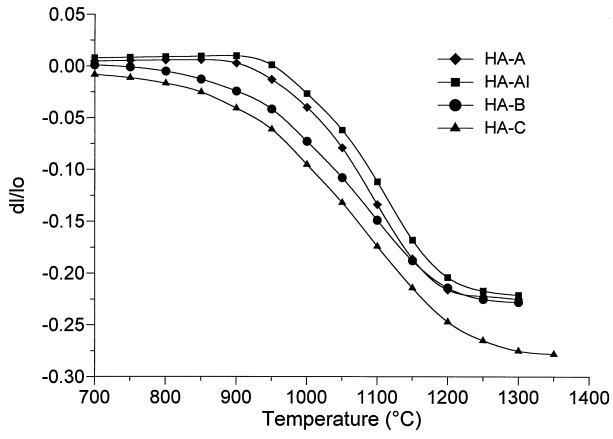

Fig. 3. Linear shrinkage of green compacts during heating at 5°C/min in dilatometer.

for HA-AI; the segments between 940 and 1100°C, which correspond to the dehydroxylation temperatures, are characterized by a rapid densification increase as expected as a consequence of such a decomposition phenomenon.[1,22] In the case of powders B and C, densification is anticipated due to the combination of two effects: the high specific surface (mainly for powder C) and the high substitution with CO_3^{2-} (mainly for powder B).[21,23,24]

Samples prepared with calcined powder AI begin to shrink at higher temperature ($T \approx 930$°C) and stop to shrink later than uncalcined ones; the total shrinkage is similar for the two powders (Fig. 3) but it occurs in a wider range of temperature. No phases arising from HA decomposition are detectable by XRD analysis in HA-A, B and C samples up to sintering temperature of 1250°C; at $T \approx 1300$°C, HA-A starts to degrade forming ≈1–2% β-TCP, which increases up to 3–4% for powder B. Anyway, such a degradation involves only the surfacial layer of the tested bars, and the peaks of β-TCP are no more detectable in the same sample after grinding (Fig. 4a). In the case of HA-C detectable degradation starts only at $T \approx 1400$°C and $Ca_4(PO_4)_2O$ (TeCP) is found among the other decomposition products (Fig. 4b).

Densification curves at various sintering temperatures were isothermally recorded for a constant time of 1.5 h as shown in Fig. 5a–c.

In Table 1, the final densities ρ_s, obtained after the isothermal treatments of the samples prepared with different powders, are reported; the green density ρ_g, the density increase during the isothermal step $\Delta\rho_{o\text{-}s}$ and final crystallinity degree X_c are also listed.

The higher surface reactivity of powder B, and even more of powder C in respect to A, can explain the rapid increase of grain growth found at low temperatures (850–940°C): in Fig. 6a–c, grain sizes of HA-A,-B, and-C bars treated at 940°C for 1.5 h are comparable even if

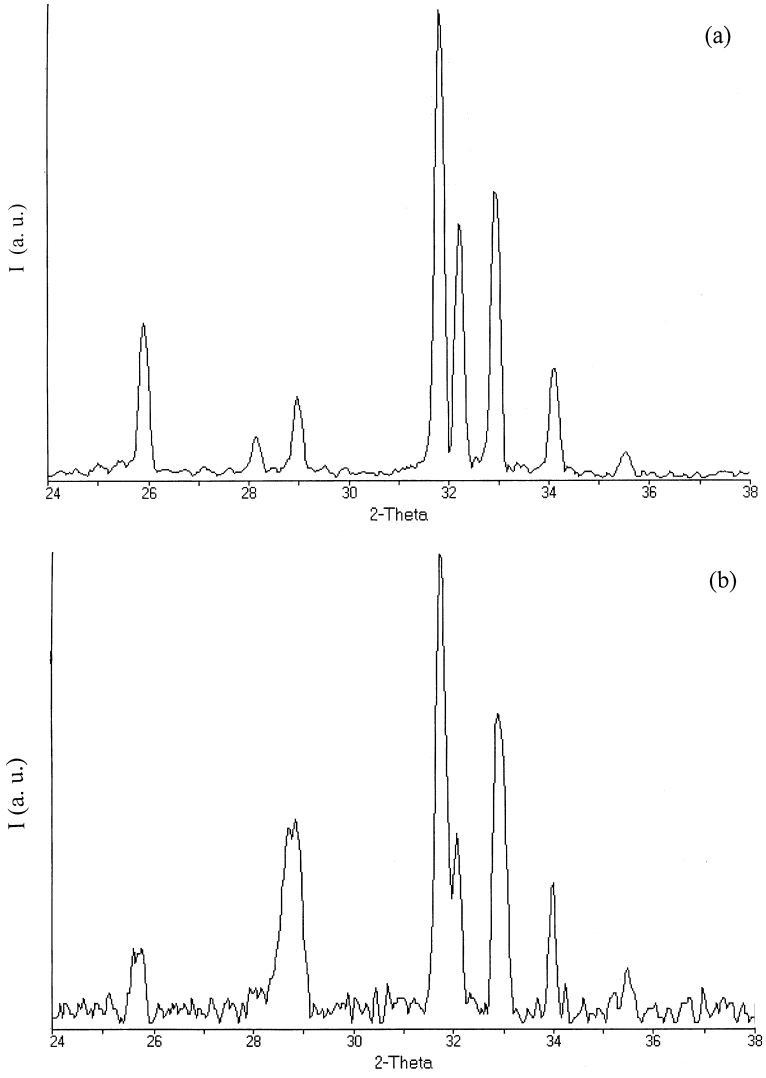

Fig. 4. XRD analysis of: powder of HA-A bar heated at 1300°C, showing absence of secondary phases (a); surface of HA-C bar heated at 1400°C, showing TeCP and other secondary phases besides HA.

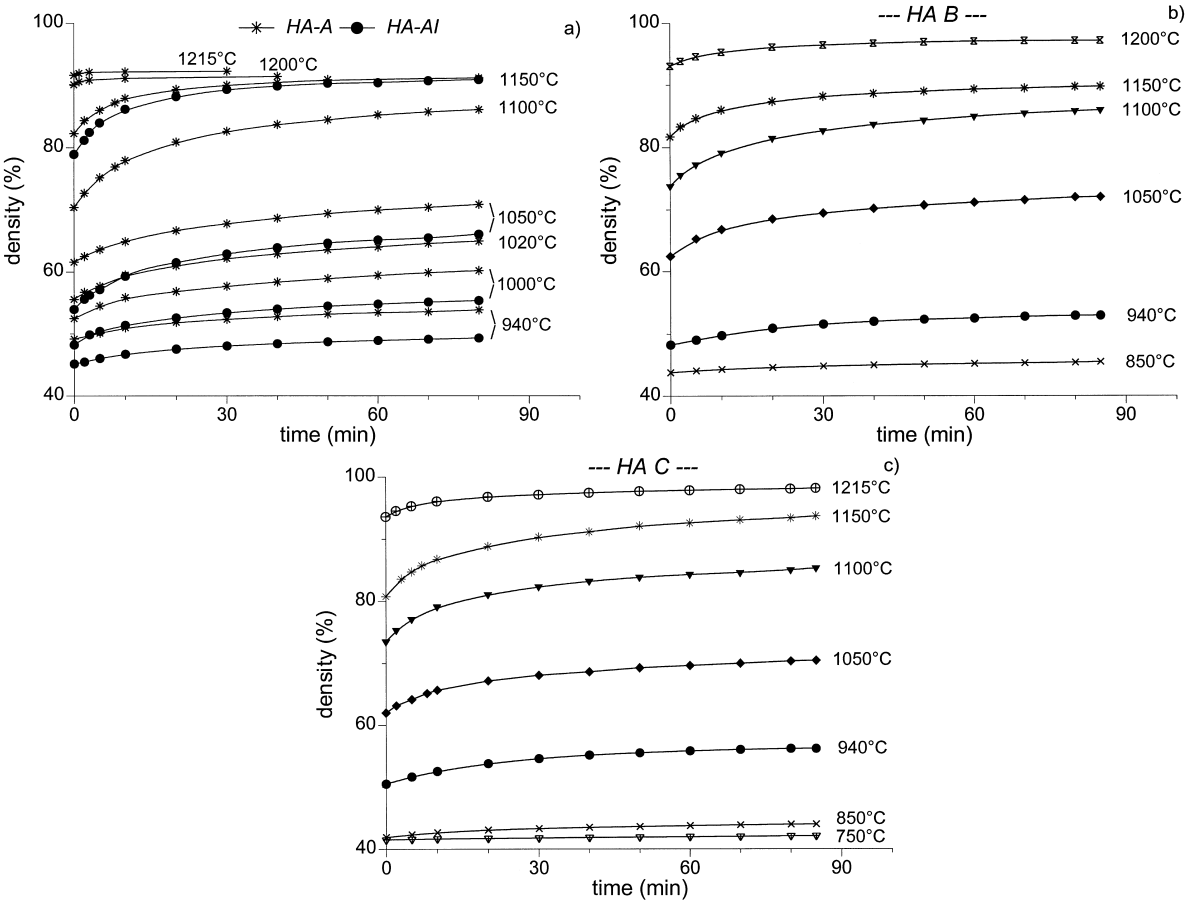

Fig. 5. Densification curves of green compacts at various sintering temperatures for 1.5 h: HA-A and HA-AI (a), HA-B (b), HA-C (c).

Table 1
Densification data of samples of HA-A,-Al,-B,-C[a]

	T_s(°C)	750	850	940	1000	1020	1050	1100	1150	1200	1215
HA A	ρ_o (%)	–	–	49	52.5	55.6	61.6	70.4	82.3	90.1	91.6
ρ_g=46% X_c=85%	ρ_s (%)	–	–	54	60	65	71	86.6	91.3	91.5	92.3
	$\Delta\rho_{o-s}$ (%)	–	–	5	7.5	9.5	9.5	16	9	1.4	0.7
	X_c (%)	–	–	85	85	90	90	92	92	95	95
HA AI	ρ_o (%)	–	–	45.1	48.2	–	54	–	79	–	–
ρ_g=45% X_c=90%	ρ_s (%)	–	–	49.3	55.4	–	66.1	–	91	–	–
	$\Delta\rho_{o-s}$ (%)	–	–	4.2	7.2	–	12.1	–	12	–	–
	X_c (%)	–	–	90	90	–	92	–	98	–	–
HA B	ρ_o (%)	–	43.8	48.2	–	–	62.4	73.8	–	–	93
ρ_g=42% X_c=45%	ρ_s (%)	–	45.5	52.9	–	–	72	86	89.7	–	96.2
	$\Delta\rho_{o-s}$ (%)	–	1.7	4.7	–	–	9.6	12.2	8	–	3.2
	X_c (%)	–	85	90	–	–	90	90	90	–	92
HA C	ρ_o (%)	41.5	41.9	50.5	–	–	62	73.5	80.7	–	93.6
ρ_g=40% X_c=20%	ρ_s (%)	42.1	44	56.3	–	–	70.3	85.3	93.7	–	98.2
	$\Delta\rho_{o-s}$ (%)	0.6	2.1	5.8	–	–	8.3	11.8	13	–	4.6
	X_c (%)	65	80	90	–	–	93	95	95	–	95

[a] ρ_g, green density; T_s, temperature of the isothermal treatment of sintering; ρ_o, density at the start (t=0) of the isothermal treatment of sintering; ρ_s, density at the end (t=1.5 h) of the isothermal treatment of sintering; $\Delta\rho_{o-s}$, increase in density due to the isothermal treatment of sintering; X_c, crystallinity degree.

particle size of the starting powders was markedly different. In spite of the acceleration in grain growth, the low crystallinity degree of powder C and B makes the driving force for densification stronger than in the case of powder A, due to the low activation energy for grain boundary movement aimed to the reduction of its total extension. At $T=850°C$, in turn, the densification extent is even higher for powder B in respect to C, in agreement with the specific chemical features of the two powders: powder B has a higher substitution with CO_3^{2-} groups which is considered[7,23,24] (at least for the fraction substituting the PO_4^{3-} groups) to lower the activation energy for particle surfacial diffusion (the substitution of 3 wt.% is enough to decrease the densification temperature of about 100°C).

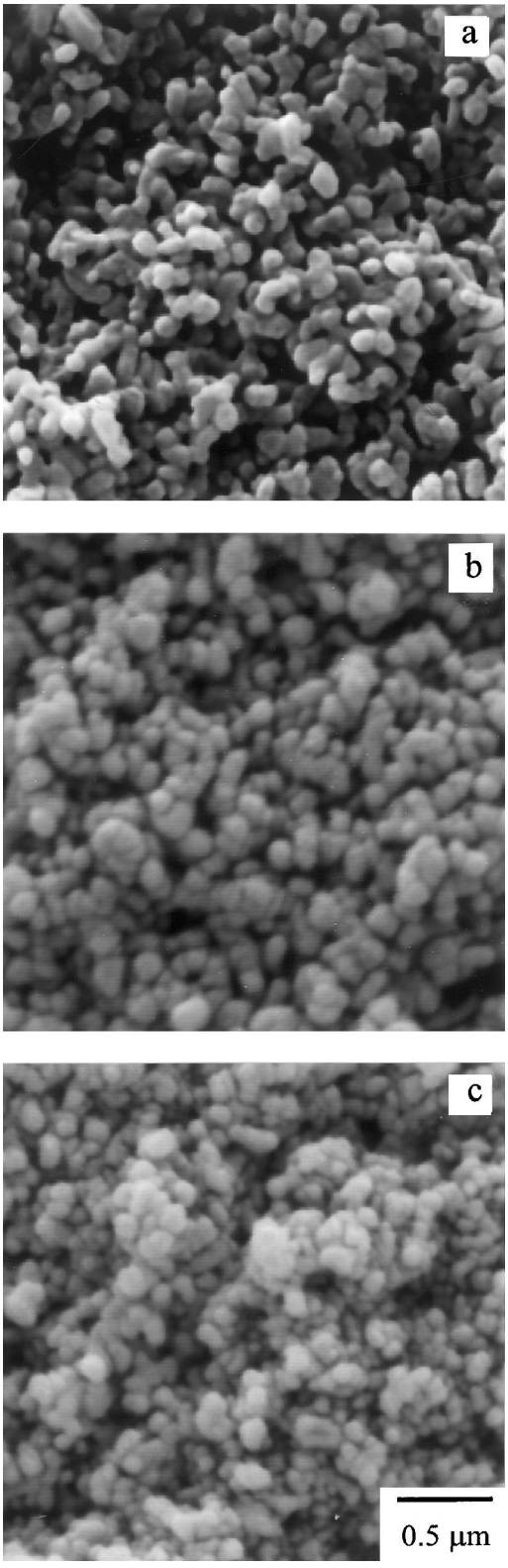

Fig. 6. Fracture morphology of HA-A (a), HA-B (b), HA-C (c) samples after sintering at 940°C for 1.5 h.

The evaluation of the crystallite sizes by XRD, evidences differences in crystallite shape, arising from a preferential size development in the basal or axial direction: HA-A sintered at 1215°C has crystallites of 740×580 Å (basal×axial) on the pellet surface and of 2050×3450 Å (basal×axial) in the powdered sample. HA-C sample sintered at 1215°C shows smaller and more isotropic crystallite size of 920 Å x 900 Å (basal×axial) in the powdered state. Since grain and crystallite size seem to proceed at the same rate, we can state that for HA-A at high temperature the reduction of total surface energy leads to an unfavourable value in the sintering driving force which stops densification beforehand; on the contrary HA-C has a densification end-point shifted ahead.

In the case of calcined powder AI the slighter slope of the curve in Fig. 3 is the consequence of a sintering in a wider range of temperature that decreases the probability of grain growth, promoting densification, although the driving force for the sintering process is somewhat sacrificed.[6,25,26] In fact, the other powders, finer than AI, should be more reactive and provide more surface as a driving force for densification; consequently the density ρ_o, at the starting of isothermic step, is lower for HA-AI than for HA-A but the increase in density $\Delta\rho_{o\text{-}s}$ during the isotherm is higher for HA-AI than for HA-A, so that both samples show a final density ≈91% after 1.5 h at 1150°C (Fig. 5a).

In Fig. 7a–d, logarithmic plots of the shrinkage dL/Lo vs. sintering time for HA-A, -B, -C and -AI samples are shown. The curves in Fig. 7a have been mathematically elaborated and it was found that the model equation

$$\text{Log } dL/Lo = \text{cost} + \text{Log}t^n$$

describes the densification mechanism for powder HA-A which is temperature and time dependent for $T \leqslant 1000°C$. In the various stages the exponent n, represented by the slope of the linear segments, assumes different values depending on the active densification mechanism. A trend can be recognized for n values in the range of temperature 940–1020°C: the second stage at lower temperature approaches the behaviour observed in the first stage at higher temperature. At $T=940°C$ the

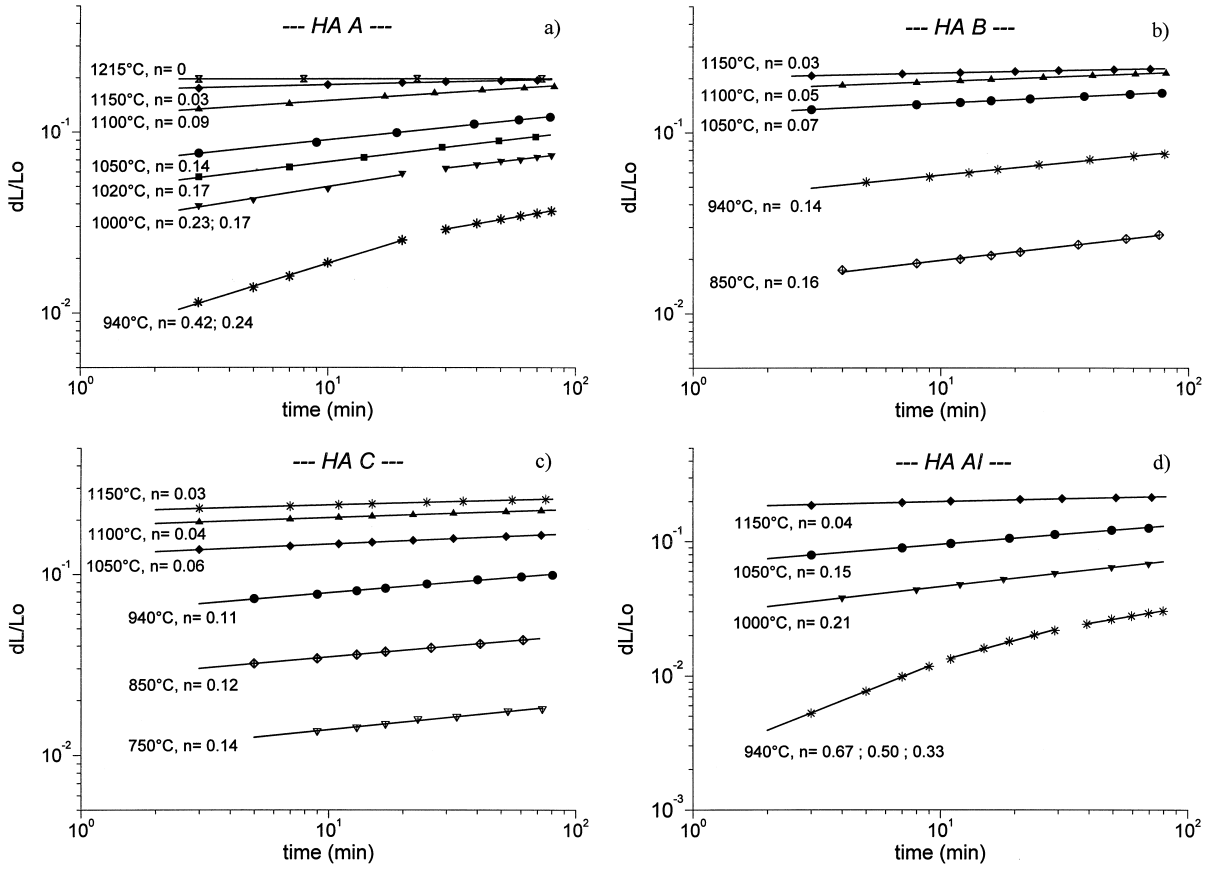

Fig. 7. Logarithmic plot of the shrinkage dL/L_o vs. sintering time at various temperature: HA-A (a), HA-B (b), HA-C (c), HA-AI (d).

rearrangement stage is missing and n value results 0.42 for the first segment, which stands for a mechanism of bulk diffusion.[8,27] For longer time n becomes 0.24 corresponding to the theoretical value for grain boundary diffusion. This value is maintained in the first stage at 1000°C and n becomes 0.17 for time > 30 min, exactly the same value found at 1020°C. The slopes of the segments are dependent on the starting powder features as well as on the degree of densification actually obtained: for density above 85% of the theoretical value, the shrinkage slope cannot represent a rate controlling mechanism and such a flattening of the curves is explained by the effect of grain growth occurring simultaneously with densification.

The microstructural evolution from 1000 to 1215°C (Fig. 8a–e) is well consistent with this interpretation; cohalescence phenomenon begins at 1050°C and strongly increases at 1100°C; at $T > 1100$°C relevant grain growth is detected: morphology appears as a continuous media with residual porosity at the triple points; at $T = 1215$°C grain growth becomes huge and porosity tends to disappear.

The logarithmic plots in Fig. 7b and c relative to HA-B and HA-C, show single segments for each sintering temperature, characterized by n values lowering with the decreasing of the starting powder crystallinity degree. At $T = 850$°C n is 0.16 and 0.12 and at $T = 940$°C n is 0.14 and 0.11 for HA-B and HA-C, respectively; at 1100°C n value decreases from 0.09 to 0.05 to 0.04 moving from HA-A to-B to-C.

The crystallinity degree of HA-A samples increases (from the starting value 80% of the green powder) with increasing sintering temperature and becomes 95% after 1.5 h at 1200°C; but X_c increases more rapidly with sintering temperature in samples prepared with low crystallinity powders, up to exceed the corresponding value of HA-A samples (Table 1). Besides the above mentioned factors, the crystallinity degree of the starting powders directly influences the densification behaviour and kinetic: as much lower is the crystallinity degree of the starting powder (i.e. powder C), as the activation energy for grain boundary diffusion is lowered; in fact, the grain boundary moves with the aim of reducing its total extension influencing grain growth rate.[23] This phenomenon, driven by cation diffusion and aimed to reduce the free enthalpy of the particles, should have an activation energy two or three times lower than the case in which recrystallization is not contemporary to sintering.[24] Actually the activation energy, evaluated in the range of temperature 940–

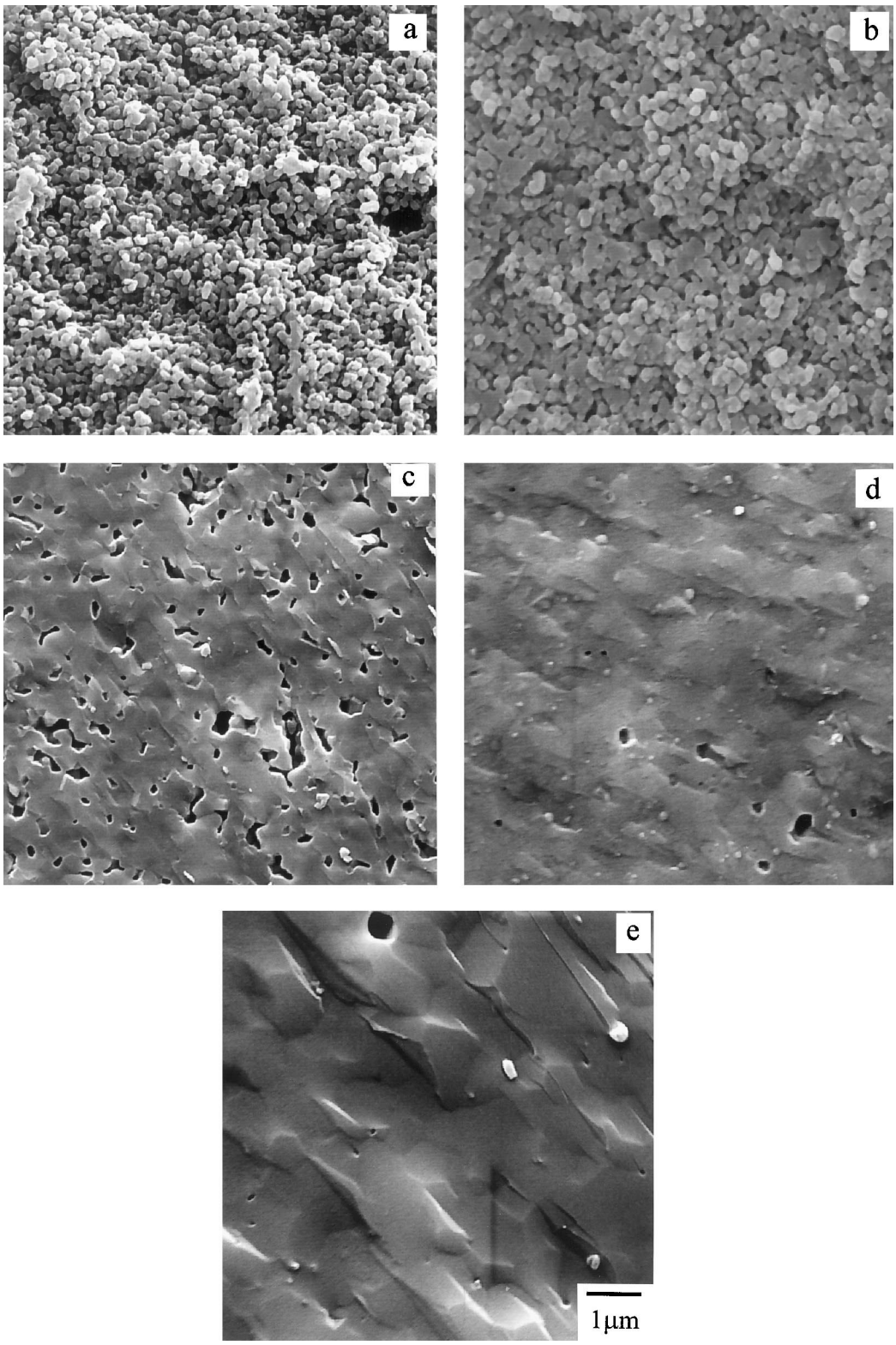

Fig. 8. Fracture image of HA-A samples after sintering for 1.5 h at: 1000°C (a), 1050°C (b), 1100°C (c), 1150°C (d), 1215°C (e).

1100°C, resulted decreasing in the order A > B > C, being ≈180, ≈130 and ≈90 KJ/mol, respectively. The increase of X_c during the sintering treatment is responsible for the low n values found in the case of HA-B and HA-C samples at each sintering temperature. In fact, such low n values do not simply relate to the densification mechanism but represent a combination of simultaneous phenomena and so easily lead to a

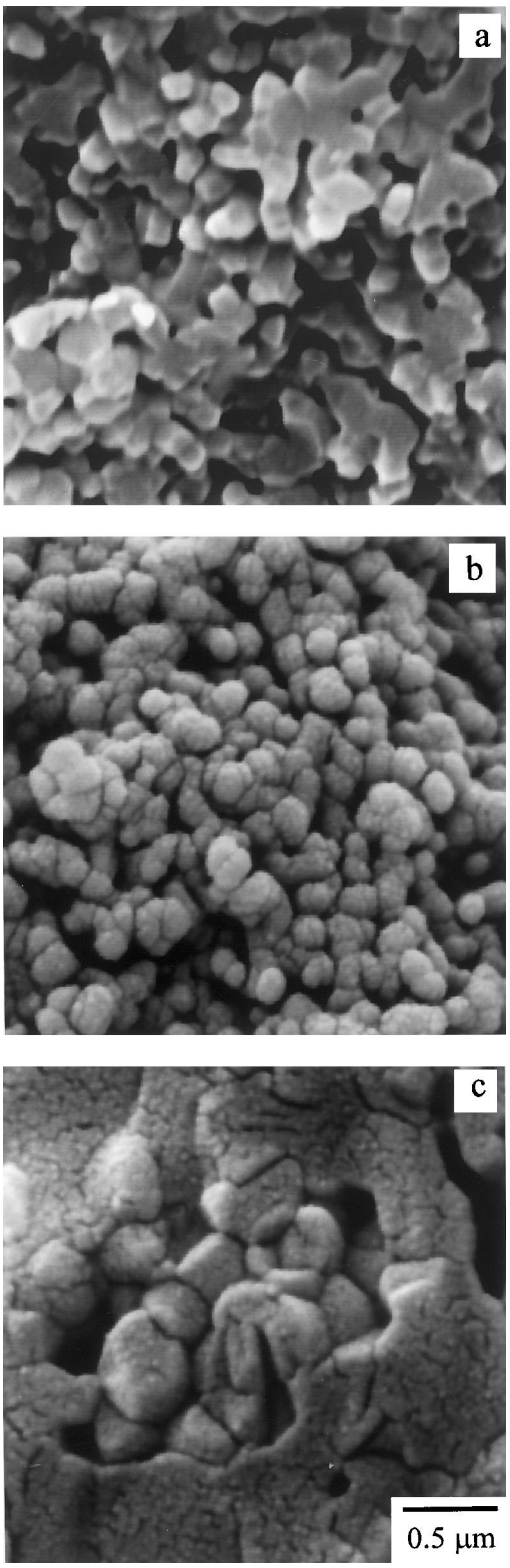

Fig. 9. Fracture image of samples after 1.5 h-sintering: HA-A at 1050°C (a), HA-C at 1050°C (b), HA-C at 1150°C (c).

misidentification of the rate controlling mechanism. HA-C sintered at 1050°C shows smaller grains and a diffuse nucleation in respect to HA-A (Fig. 9a and b); at higher temperature coalescence phenomenon and again

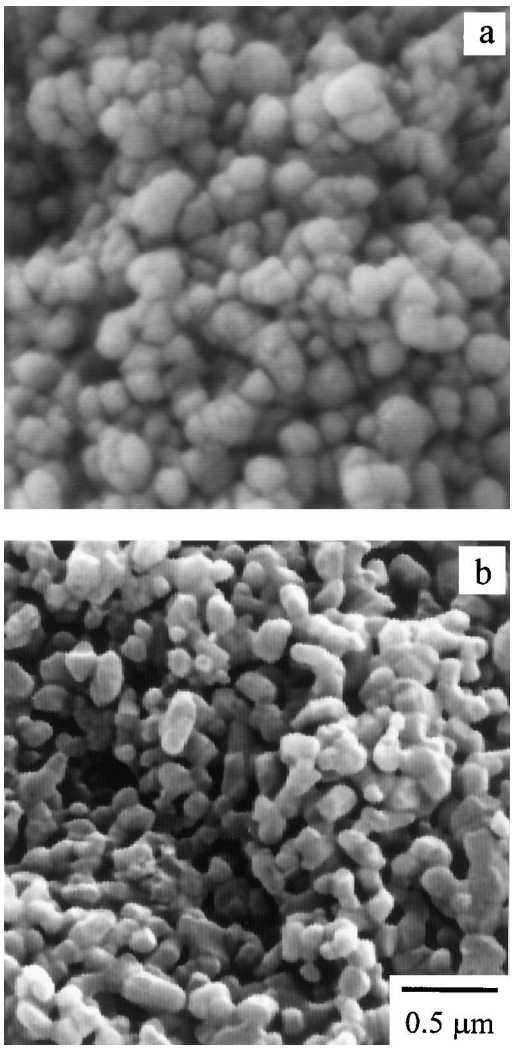

Fig. 10. Fracture morphology of samples sintered at 1000°C for 1.5 h: HA-A (a), HA-AI (b).

diffuse nucleation are well observed on grains of both HA-B and HA-C (Fig. 9c).

The logarithmic plot (Fig. 7d) of HA-AI samples is characterized by n values higher than those of uncalcined powder: at $T=940$°C, three linear segments decreasing in slope, $n \approx 0.67$, 0.50, 0.33, fit the data as the sintering time increases. $n=0.67$ could be related to the process of particle rearrangement, which is not found in the case of the corresponding uncalcined HA-A sample; $n=0.50$ is consistent with a rate controlling mechanism of bulk diffusion parallel to the interparticle centerline through the area of the interparticle flat surfaces and $n=0.33$ can be correlated with both mechanisms of bulk and grain-boundary diffusion.[8,28]

After sintering at 940–1000°C, HA-AI samples show grains more rounded and with coalescence markedly reduced in respect to HA-A treated at the same temperature (Fig. 10a, b); such a result is in agreement with the above mentioned delaying effect on sintering due to the calcination pretreatment of powder.

4. Conclusions

Three different HA powders with starting crystallinity from 20 to 80% were prepared and their sintering kinetic carefully studied.

The physico-chemical features of the different powders (grain size, crystallinity degree, chemical substituting groups, etc) drive the densification behaviour and kinetic: grain growth is strongly stimulated in HA-B and HA-C due to grain boundary diffusion process, which improves densification in respect to powder A and AI.

A temperature and time dependent kinetic was recognized for HA-A: at $T \approx 940°C$, a mechanism of bulk diffusion is hypothesized, followed by grain boundary diffusion mechanism for time longer than 30 min.

Calcination treatment (HA-AI) has a delaying effect on sintering at low temperature: at temperatures in the range 940–1000°C grains are more rounded and coalescence is reduced, that agrees with n values higher in respect to HA-A and the possibility to identify a preceding mechanism of particle rearrangement; but, at higher temperature, decreasing the probability of grain growth, the densification is improved.

Besides the grain smallness (high reactivity) and the high thermal stability (no formation of low-density phases), the low crystallinity degree of the starting powder highly favours the densification process. As a consequence the low n values found for HA-B and HA-C, especially for $T > 850°C$, cannot represent a rate controlling mechanism, being the result of several simultaneous phenomena occurring during sintering treatment.

References

1. Wang, P. E. and Chaki, T. K., Sintering behaviour and mechanical properties of hydroxyapatite and dicalcium phosphate. *J. Mat. Sci.: Mat. Med.*, 1993, **4**, 150–158.
2. Van Landuyt, P., Li, F., Keustermans, J. P., Streydio, J. M. and Delannay, F., The influence of high sintering temperature on the mechanical properties of hydroxyapatite. *J. Mat. Sci.: Mat. Med.*, 1995, **6**, 8–13.
3. Arita, I. H., Castano, V. M. and Wilkinson, D. S., Synthesis and processing of hydroxyapatite ceramic tapes with controlled porosity. *J. Mat. Sci.: Mat. Med.*, 1995, **6**, 19–23.
4. Zhou, J., Zhang, X., Chen, J., Zeng, S. and De Groot, K., High temperature characteristic of synthetic hydroxyapatite. *J. Mat. Sci.: Mat. Med.*, 1993, **4**, 83–85.
5. Zyman, Z., Cao, Y. and Zhang, X., Periodic crystallization effect in the surface layers of coatings during plasma spraying of hydroxyapatite. *Biomaterials*, 1993, **14**, 1140–1144.
6. Wang, C. K., Ju, C. P. and Chern Lin, J. H., Effect of doped bioactive glass on structure and properties of sintered hydroxyapatite. *Mat. Chem. Phys*, 1998, **53**, 138–149.
7. Suchanek, W. and Yoshimura, M., Processing and properties of hydroxyapatite-based biomaterials for use as hard tissue replacement implants. *J. Mater. Res.*, 1998, **13**, 94–117.
8. Lynn Johnson, D. and Cutler, I. B., Diffusion sintering: I, Initial stage sintering models and their application to shrinkage of powder compacts. *J. Am. Ceram. Soc.*, 1963, **46**, 541–545.
9. Ruys, A. J., Brandwood, A., Milthorpe, B. K., Dickson, M. R., Zeigler, K. A. and Sorrell, C. C., The effects of sintering atmosphere on the chemical compatibility of hydroxyapatite and particulate additives at 1200°C. *J. Mat. Sci.: Mat. in Med.*, 1995, **6**, 297–301.
10. Kijima, T. and Tsutsumi, M., Preparation and thermal properties of dense polycrystalline oxyhydroxyapatite. *J. Am. Ceram. Soc.*, 1979, **62**, 455–460.
11. Jarcho, M., Bolen, C. H., Thomas, M. B., Bobick, J., Kay, J. F. and Doremus, R. H., Hydroxylapatite synthesis and characterization in dense polycrystalline form. *J. Mat. Sci.*, 1976, **11**, 2027–2035.
12. Han, Y., Xu, K., Lu, J. and Wu, Z., The structural characteristics and mechanical behaviors of nonstoichiometric apatite coatings sintered in air atmosphere. *J. Biomed. Mater. Res.*, 1999, **45**, 198–203.
13. Kamiya, K., Yoko, T., Tanaka, K. and Fujiyama, Y., Growth of fibrous hydroxyapatite by the hydrolysis of brushite. *J. Mat. Sci.*, 1989, **24**, 827–832.
14. Monma, H. and Kamiya, T., Preparation of hydroxyapatite by the hydrolysis of brushite. *J. Mat. Sci.*, 1987, **22**, 4247–4250.
15. Ishikawa, K., Ducheyne, P. and Radin, S., Determination of the Ca/P ratio in calcium-deficient hydroxyapatite using X-ray diffraction analysis. *J. Mat. Sci.: Mat. in Med.*, 1993, **4**, 165–168.
16. Li, Y., De Groot, K., De Wijn, J., Klein, C. P. A. T. and Meer, SV.D., Morphology and composition of nanograde calcium phosphate needle-like crystals formed by simple hydrothermal treatment. *J. Mat. Sci.: Mat. in Med.*, 1994, **5**, 326–331.
17. De Groot, K., Bioceramics consisting of calcium phosphate salts. *Biomat*, 1980, **1**, 47–50.
18. Doi, Y., Koda, T., Adachi, M., Wakamatsu, N., Goto, T., Kamemizu, H., Moriwaki, Y. and Suwa, Y., Pyrolysis-gas chromatography of carbonate apatites used for sintering. *J. Biomed. Mater. Res.*, 1995, **29**, 1451–1457.
19. Ellies, L. G., Nelson, D. G. A. and Featherstone, J. D. B., Crystallographic structure and surface morphology of sintered carbonated apatites. *J. Biomed. Mater. Res.*, 1988, **22**, 541–553.
20. Tampieri, A., Celotti, G., Sprio, S. and Mingazzini, C., Characteristics of synthetic hydroxyapatites and attempts to improve their thermal stability. *Mat. Chem. Phys*, 2000, **64**, 54–61.
21. Bossert, J., Fidancevska, E., Bucker, M. and Milosevski, M., Sintering and properties of dense and porous $Ca_3(PO_4)_2$. *Sci. Sinter.*, 1998, **30**, 19–27.
22. Cihlar, J., Buchal, A. and Trunec, M., Kinetics of thermal decomposition of hydroxyapatite bioceramics. *J. Mat. Sci.*, 1999, **34**, 6121–6131.
23. Boiko, Y. and Worch, H., Grain growth in nanocrystalline materials. *Sci. Sinter.*, 1999, **31**, 151–155.
24. Vassen, R., Stöver, D. and Uhlenbusch, J., Sintering and grain-growth of ultrafine amorphous SiC–Si-powder mixtures. In *Euro-Ceramics II, Vol. 2, Structural Ceramics*, ed. G. Ziegler and H. Hausner. 1991, p. 791.
25. Petzow, G., Exner, H. E., Particle rearrangement in solid state sintering. In *Sintering, Key Papers* (EN843-2). Advanced Technical Ceramics, pp. 611–618.
26. Juang, H. Y. and Hon, M. H., Effect of calcination on sintering of hydroxyapatite. *Biomat*, 1996, **17**, 2059–2064.
27. Kuczynski, G. C., Towards the understanding of the process of sintering. In *Sintering '85*, ed. G. C. Kuczynski, D. P. Uskokovic, H. Palmour III and M. M. Ristic. Plenum Press, New York, 1987, pp. 3–16.
28. Moon, I. H., Lee, J. S. and Ahn, I. S., The dependence of sinterability of Ni-added W-powder compact on the contact neck size of W-particles. In *Sintering 85*, ed. G. C. Kuczynski, D. P. Uskokovic, H. Palmour III and M. M. Ristic. Plenum Press, New York, 1987, pp. 143–153.